Nuclear Instruments and Methods in Physics Research A 1082 (2026) 170917

Contents lists available at ScienceDirect

Nuclear Inst. and Methods in Physics Research, A

journal homepage: www.elsevier.com/locate/nima

Full Length Article

Radiation effects of CERN-PS 24 GeV/c protons in silicon strip sensors, evaluated with ATLAS18 ITk strip sensor test structures☆

I. Mandić [a,*], V. Cindro [a], M. Mikuž [a,b], B. Novak [a], P. Federičová [c], R. Jirásek [c], J. Kroll [c], J. Kvasnička [c], M. Mikeštíková [c], P. Tůma [c], V. Fadeyev [d], Y. Unno [e], E. Bach [f], C. Fleta [f], M. Ullan [f], U. Soldevila [g], R.S. Orr [h], C.K. Mahajan [h], S.K. Sridhar [h], A.S. Chisholm [i], I. Dawson [j]

[a] Jožef Stefan Institute, Jamova 39, 1000, Ljubljana, Slovenia
[b] Faculty of Mathematics and Physics, University of Ljubljana, Jadranska ulica 19, 1000, Ljubljana, Slovenia
[c] Institute of Physics, Academy of Sciences of the Czech Republic, Na Slovance 2, 18200, Prague 8, Czech Republic
[d] Santa Cruz Institute for Particle Physics (SCIPP), University of California, Santa Cruz, CA 95064, USA
[e] Institute of Particle and Nuclear Study, High Energy Accelerator Research Organization (KEK), 1-1 Oho, Tsukuba, Ibaraki 305-0801, Japan
[f] Instituto de Microelectrónica de Barcelona (IMB-CNM), CSIC, Campus UAB-Bellaterra, 08193, Barcelona, Spain
[g] Instituto de Física Corpuscular, IFIC/CSIC-UV, C/Catedrático José Beltrán 2, E-46980, Paterna, Valencia, Spain
[h] Department of Physics, University of Toronto, 60 Saint George St., Toronto, Ontario M5S1A7, Canada
[i] School of Physics and Astronomy, University of Birmingham, Birmingham, B1 52TT, United Kingdom
[j] Particle Physics Research Centre, Queen Mary University of London, G.O. Jones Building, Mile End Road, London, E1 4NS, United Kingdom

ARTICLE INFO

Keywords:
Silicon strip detectors
Charge collection
Radiation hardness

ABSTRACT

Test structures from the ATLAS18 ITk strip detector wafers were irradiated with 24 GeV/c protons. These test structures were positioned at various angles with respect to the proton beam. Blocks of G10 material were placed in front of these test structures to study the effect of scattering of primary protons on the received particle fluence. The results confirm that both the incidence angle of the beam and scattering significantly influence the actual fluence to which the samples are exposed. Miniature strip detectors, first irradiated with protons, were also irradiated with reactor neutrons, to a combined fluence of $\Phi_{neq} = 1.6 \times 10^{15}$ cm^{-2}. The combination of proton and neutron fluences matched the combination expected in the most exposed part of the strip detector in the ALTAS Inner Tracker (ITk). Good charge collection was measured confirming that the strip detectors are sufficiently radiation hard for successful operation to highest fluences expected at the HL-LHC.

1. Introduction

The silicon strip detectors in the Inner Tracker (ITk) [1] of the upgraded ATLAS experiment at HL-LHC will have to operate in a high radiation environment. The strip sensor region of the tracker has to withstand irradiation with a 1 MeV neutron equivalent fluence[1] of $\Phi_{neq} = 1.6 \times 10^{15}$ cm^{-2}. To verify such radiation hardness, extensive irradiation studies were performed during development of these sensors. These included irradiations with reactor neutrons as well as protons with 25 MeV and 70 MeV kinetic energy and 24 GeV/c momentum[2] [2–4]. During four years of production of more than 25 000 sensors for the ITk, regular irradiations of test structures with neutrons and low energy protons are a part of the production quality assurance (QA) procedures [5]. The Collected Charge (CC) after irradiation is one of the QA parameters, with a minimum requirement of 6350 electrons[3] at a bias voltage of 500 V (the maximum bias voltage for ITk strips detector). Because of less frequent availability, irradiations with high energy protons are not part of the QA procedures, but irradiation campaigns with 24 GeV/c protons at CERN PS were carried out to check the effect of high energy hadrons on samples from production wafers.

* Corresponding author.
E-mail address: igor.mandic@ijs.si (I. Mandić).
[1] The 1 MeV neutron equivalent fluence (neq) is used to express the fluence of different particles in terms of the damage caused by 1 MeV neutrons, based on the amount of Non-Ionizing Energy Loss (NIEL) they produce.
[2] 23 GeV kinetic energy.
[3] The value was chosen after optimization of yield of the sensors in the distributions of collected charge, breakdown voltage, and signal-to-noise ratio >10.

https://doi.org/10.1016/j.nima.2025.170917
Received 15 January 2025; Received in revised form 28 July 2025; Accepted 29 July 2025
Available online 7 August 2025

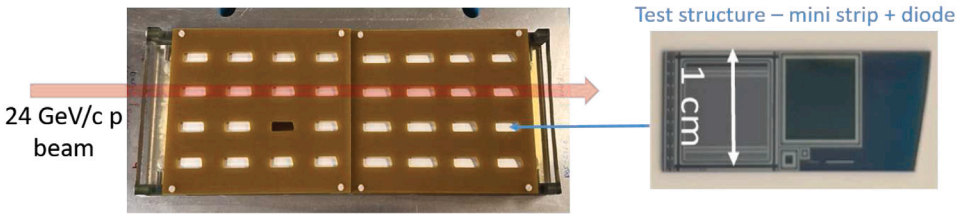

Fig. 1. A photo of the mechanical support used in irradiations is shown on the left. The test structure called mini&MD8 on the right contains a mini strip detector (1 × 1 cm^2) and a diode (0.8 × 0.8 cm^2). The test structures were placed in holders in the support structure machined in the 6 mm thick G10 material. The red arrow in the left figure represents the direction of 24 GeV/c proton beam. The incidence angle of the beam on the test structure was ∼1.45°.

Radiation damage to the sensor bulk is the consequence of the displacement of lattice atoms. It is known that the effect of irradiation on properties of silicon detectors may depend on irradiation particle type even at the same NIEL. For example, the change of full depletion voltage after irradiation with 24 GeV/c protons is different than after irradiation with reactor neutrons in detectors produced on silicon with high oxygen content [6,7]. In the upgraded ATLAS experiment displacement damage will be caused by charged hadrons and neutrons [1,8]. In the most exposed part of the ITk strip detector, charged hadrons and neutrons will contribute roughly equally to the NIEL, while in other regions neutrons will dominate. Among the available charged hadron radiation sources, bulk damage caused by 24 GeV/c protons most closely resembles the damage expected from charged hadrons in the upgraded ATLAS experiment, which are mostly protons and pions with energies of a few hundred MeV. It is therefore important to check the performance of detectors after irradiation with 24 GeV/c protons.

Previous irradiation tests, including tests with 24 GeV/c protons, showed good performance after irradiation for several versions of ITk strip detector prototypes [2–4]. However, after some of the recent irradiations of samples from the ATLAS18 production strip sensors with 24 GeV/c protons to $\Phi_{neq} \sim 1.6 \times 10^{15}$ cm^{-2}, the CC at a bias voltage of 500 V was below the QA acceptance level of 6350 electrons.[4] These results initiated extensive irradiation, measurement, and simulation work to understand the causes of the low CC using the test structures from the wafers of the ATLAS18 production sensors [5,9,10].

2. Irradiations

Irradiations with 24 GeV/c protons were performed at the IRRAD test facility at CERN [11,12]. The proton beam at IRRAD, for the irradiations described in this work, is narrow and has a roughly Gaussian intensity profile with a Full Width at Half Maximum in the x direction FWHM$_x$ = 7.8 mm and FWHM$_y$ = 9.7 mm as determined using the Beam Profile Monitor [11,12]. In irradiations described in this work, samples were not "scanned in the beam" but they were instead positioned in the beam and kept at a fixed position until the final fluence was reached.

2.1. The earlier experiments in 2021 and 2022

The test structure called mini&MD8 contains a mini strip detector and a pad diode on a single piece of silicon with size of roughly 1 × 2 cm^2 - see Fig. 1. To irradiate a structure of this size, without scanning, it was placed in the narrow beam at a shallow angle of ∼ 1.45° with respect to the beam direction. The mechanical support was made of G10 material in which place holders were machined as shown in Fig. 1. Several samples were placed one behind the other in the beam direction and irradiated together. This resulted in thick layers of G10 and silicon materials on which primary protons scattered and generated showers of secondary particles. Geant4 simulations indicated that, in such a setup, secondary particles originating from the G10 or/and silicon of irradiated devices, due the shallow incidence angle, increase the effective fluence. Irradiations of ATLAS18 samples with this type of setup were carried out in the years 2021 and 2022. In both experiments significantly lower charge collection efficiency than expected was measured at high fluences, possibly because the actual fluence was larger than anticipated.

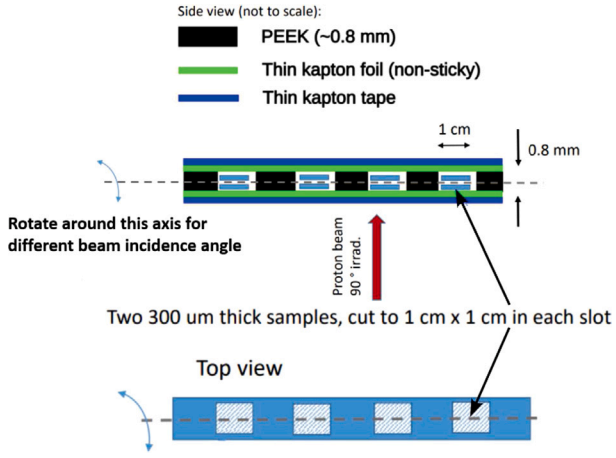

Fig. 2. Drawing of the sample holder.

2.2. The experimental setup of this work in 2023

Mini strip detectors (mini), pad diodes (MD8) and Test-Chips (TC) containing various test circuits [9] were irradiated for the study of effects of scattering and irradiation angle. All samples were cut to 1 × 1 cm^2 size from larger ITk strip test structures. Mini strip detectors and MD8 diodes were cut from the structure shown in Fig. 1 while Test-Chips were cut from a different type of test structure (see [10]).

Samples were fixed to light weight holders made of a thin layer of PEEK (PolyEther Ether Ketone) plastic shown in the drawing in Fig. 2. Twelve holders, each holding two samples in each of the four slots, were mounted at different angles to the direction of the proton beam as shown in Fig. 3. Two sets of four holders were mounted at angles 90°, 12°, 6° and 1.5°. The first set contained pairs of mini strip sensors in each slot and the second set a Test Chips (TC) and a MD8 pad diodes in each slot. Blocks of G10 material were placed in front of the last four holders mounted at 90° and 1.5°. The samples were arranged in four columns separated by 2.4 cm. Each of the columns was centred in the proton beam and kept at fixed position (there was no scanning) during irradiation. After the irradiation of one column was finished, the next column was moved into the beam. Simulations, which will be described in the next section, showed that the fluences delivered to the samples in neighbouring columns are below 1% of fluence for samples on the eight holders before G10 scattering blocks and less than 4% for the last four holders behind the blocks. The target Φ_{neq} for columns 1 to 4 (see

[4] See Fig. 13, symbols A18(PS2021) and A18(PS2022) and comments in Sections 4.2 and 5.

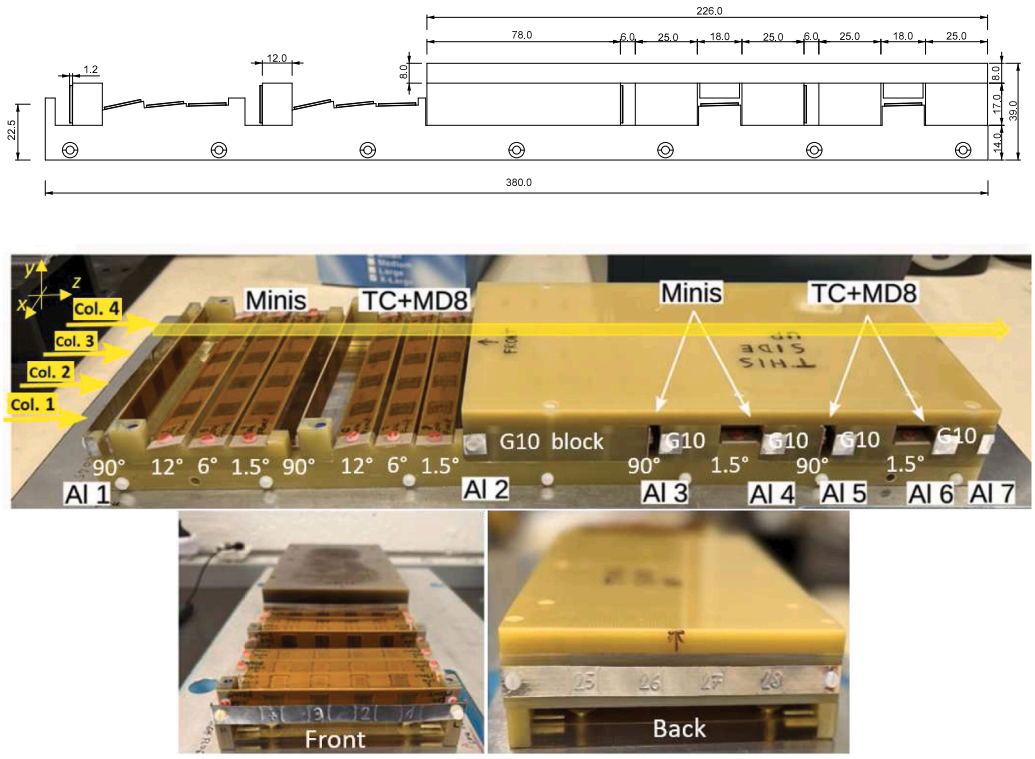

Fig. 3. Drawing of side view (top) and photos of the irradiation setup. Pairs of Mini strip (Minis) detectors were mounted on the first four lightweight holders, while pairs of one Test Chip and one MD8 diode (TC+MD8) were mounted on the next four holders. The holders were positioned at different angles with respect to the beam direction — these angles are indicated on the photo. Test structures were also placed behind blocks of G10 material to study the effect of secondary particles generated by scattering of primary protons. Samples on the holders were arranged in four columns, each exposed to a different proton fluence. Seven layers of aluminium foil, labelled Al1 to Al7 in the photo, were mounted in the setup, all at 90°, for monitoring the proton fluence.

Fig. 3) were 1×10^{14}, 5×10^{14}, 1×10^{15} and 1.6×10^{15} cm^{-2}, respectively. The fluences reached for columns 3 and 4 were significantly lower than these target values because the irradiation was stopped by the IRRAD crew for technical reasons before the target fluence was reached. The sample holder was placed in a cold box maintaining a temperature of −20 °C during irradiation.

3. Dosimetry and simulation

The proton fluence was monitored by measuring the activity of ^{22}Na and ^{24}Na in aluminium (Al) foils [13]. As shown in Fig. 3, seven layers of Al foils were installed in the setup at 90° to the beam. After irradiation 1 × 1 cm^2 pieces matching the positions of columns of samples were cut from the Al foils and their radioactivity measured. With this method the proton fluence was determined with an accuracy of 7%. The proton fluence taken from the activated foil dosimetry is converted to 1 MeV neutron equivalent fluence in silicon, Φ_{neq}, by multiplying it with a hardness factor of 0.62 [14].

The relationship between the radioactivity of Al foils and the fluence of 24 GeV/c protons is well known [13,15]. However, the relationship between the fluence of secondary particles, produced by the interactions of primary protons with the material in the setup, and the activation of Al foil is not known for all secondary particle types and energies. As a rough estimate, Φ_{neq} were calculated from the foil activity using conversion constants for 24 GeV/c protons. In the following text, this quantity is referred to as the measured fluence. The accuracy of this estimation was assessed by comparison with a Geant4 simulation and by measurements of the leakage current under reverse bias in diodes irradiated in the setup, as explained below.

Fig. 4 shows the measured Φ_{neq} for seven layers of Al foils for four irradiation columns in the setup (see Fig. 3). The striking feature of Fig. 4 is the significant increase of the measured fluence on layer 2, and even more so on layer 3, behind the first G10 scattering block in the setup compared to layer 1. This increase is attributed to the contribution of secondary particles generated in interactions of the beam with the material in the setup.

3.1. Simulation

The Geant4 simulation [16] of the experiment was made using the specifications of all particles and their interactions required to run a shielding, high energy or underground detector simulation, called "Shielding physics list" [17]. A detailed CAD drawing of the irradiation setup shown in Fig. 5a was used to describe the material distribution in the simulation. The NIEL in silicon samples was calculated by summing the path lengths of particles in Si and using the damage factors from [18–21].

Fig. 5(b) shows the NIEL relative to the NIEL in layer 1 calculated with Geant4 for the silicon samples in different layers of the setup. At the locations of Al foils in Fig. 5b the NIEL was calculated for a same size silicon sample as in the other layers (1 × 1 cm^2, 300 μm thick) positioned at 90° to the beam. It can be seen that the fluence for samples irradiated at shallow angles in layers 2, 3, 4, 6, 7 and 8 is significantly larger than the fluence of samples irradiated at 90°. This is a geometrical effect because the FWHM of the beam intensity profile is comparable with the dimension of the samples. At shallow angle a larger part of the sample is exposed to the high intensity core of the beam than in the case of exposure at 90°.

The effect of irradiation at shallow angle was also studied in a separate irradiation experiment at the CERN IRRAD facility in which aluminium foils were irradiated at 90° and at 0°. A sketch of the experiment is shown in Fig. 6. The dimension of foil F1 was 0.5 × 0.5 cm^2 while foils F2 and F3 were 1 × 1 cm^2. The fluence measured with the small foil F1 was 70% larger than the fluence measured with the

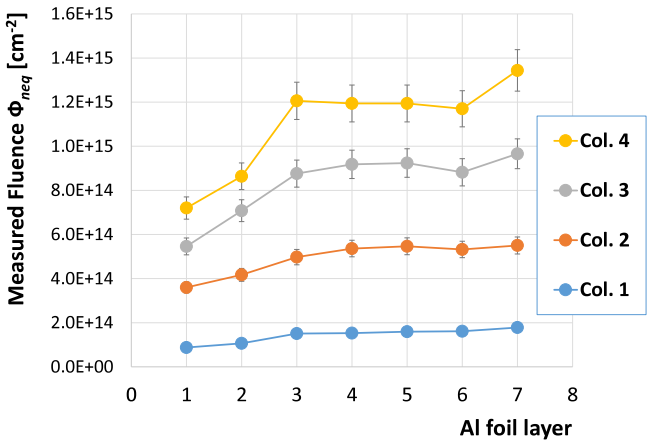

Fig. 4. The figure shows the Φ_{neq} calculated from the radioactivity of Al foils, using parameters for 24 GeV/c protons, for 28 aluminium pieces from four columns of the irradiation setup in Fig. 3.

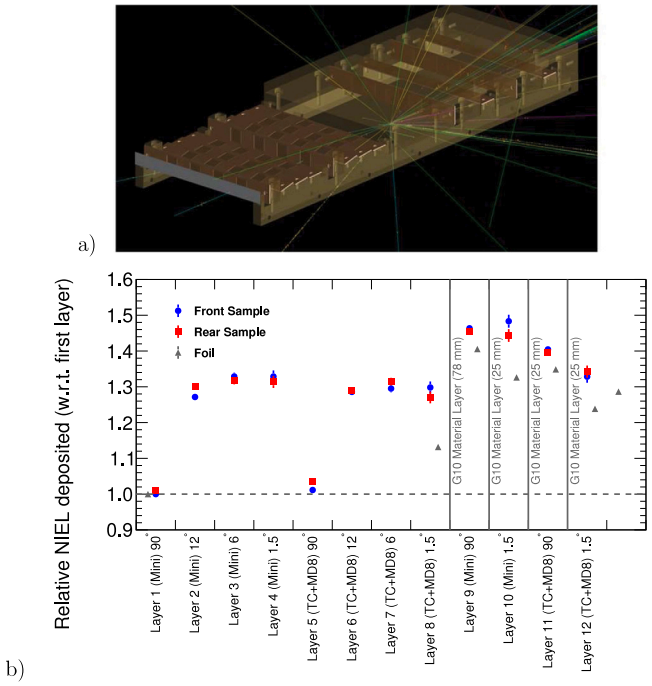

Fig. 5. (a) Drawing of the setup used in the Geant4 simulation with an event showing secondary tracks generated in an interaction of a primary proton. (b) Relative NIEL calculated by the Geant4 simulation for silicon samples at different layers. The positions correspond to different angles, as indicated in the x-axis labels. The fluence was calculated separately for two silicon samples at each position. At the locations of Al foils, the relative NIEL was calculated for 1×1 cm^2, 300 μm thick silicon positioned at 90° to the beam. These values are marked with grey triangles.

larger foil F2, confirming the higher intensity at the centre of the beam. The fluence measured with the horizontal foil F3 was 30% larger than that measured with F2 at 90°. This is consistent with the 30% increase of fluence calculated by the Geant4 simulation for samples positioned at shallow angles in layers 2, 3, 4 and 6, 7, 8 in Fig. 5(b).

The effect of the beam incidence angle in Fig. 5b is much less significant for samples in layers 9, 10, 11 and 12 with G10 scattering blocks placed between the beam and the samples. This may be expected because inelastic interactions of primary protons create many secondary particles at larger angles, effectively broadening the beam size and thus reducing the geometrical effect of a shallow angle.

It can be seen in Fig. 5b that fluences decrease with increasing layer number in these layers. The variation of fluence with position in the region containing G10 scattering blocks is governed by the generation and absorption of secondary particles, as well as by the attenuation of the primary beam, which resulted in the observed dependence. Fig. 7 shows the kinetic energy spectrum of particles incident on the sample in layer 11. The spectrum peaks at energies much lower than the beam energy, indicating that many charged particles are absorbed in the G10 before reaching the sample. Additionally, secondary particles may miss the sample if they are produced at larger angles relative to the beam direction. Simulations indicate that the differences between fluences at the sensor and aluminium foil positions, as observed in layers 9, 10, 11, and 12 in Fig. 5b, are a consequence of the geometric effect of the distance from the G10 material, due to the broad angular distribution of secondary particle directions. The ∼5 mm air gap between the sample and Al foil 3 in layer 9 results in a fluence reduction of a few percent. The effect is more pronounced in layers 10 and 12 due to larger gaps.

Fig. 8 shows measured and calculated fluences relative to the layer 1 for all layers in the setup. Measured data points are averages for four foils at each layer. The error bars show the standard deviation of these four values. Geant4 fluences were calculated for 1×1 cm^2, 300 μm thick pieces of silicon at the locations of Al foils. It can be seen that at layer 3 the measured fluence is by up to 60% larger than at layer 1, which is a large effect. There is good agreement between measurement and simulation for layer 2 while for higher layer numbers the simulation underestimates the measured values.

It should be noted that only a rough agreement is expected, despite the precise material distribution, due to a combination of factors. First, there is uncertainty in the correlation between Al foil activation and Φ_{neq} in silicon within an environment containing secondary particles. Estimating this relationship would require folding the secondary particle flux spectrum predicted by Geant4 with the relevant activation cross sections for ^{24}Na and ^{22}Na production in aluminium. However, this is not straightforward due to the limited availability of experimental cross-section data for particles other than protons [22]. Additional uncertainties include possible deviations of the true beam shape from the Gaussian profile used in the simulation. Differences may also arise from misalignments between the irradiation setup and the proton beam, which are not accounted for in the simulation.

This work does not aim to study the correlation between NIEL in silicon (measured or modelled in Geant4) and aluminium activation in detail, but rather to demonstrate that secondary particles, originating from the support structure of the irradiation setup, contribute significantly to the NIEL in silicon samples.

3.2. Estimating fluences

As shown in Fig. 3 not all samples had Al foils placed near their positions such that the fluence to which samples were exposed was estimated based on measurements and simulation. The fluence measured with Al1 is the best estimate of the fluence for samples in layer 1 and this value was used also for layer 5 (90°), because the Geant4 simulation did not show significant differences between these two layers. As mentioned at the beginning of this section, the precision of fluence measurement with the Al foil is 7%.

The simulation results in Fig. 5b show that devices irradiated at shallow angles in layers 2, 3, 4 and 6, 7, 8 were exposed to about 30% higher fluence than those in layer 1. The increase of fluence by 30% due to the shallow angle was seen also in the separate experiment shown in Fig. 6. Therefore, the fluences for sensors in these layers were estimated by multiplying the fluence of layer 1 with factors calculated using the Geant4 simulation. The uncertainty of this factor is estimated to be of the order of 10%. It arises from the imperfect beam description in the simulation.

The sensors in layers behind the G10 scattering blocks have aluminium layers in their vicinity. Al3 is located near sensor layer 9, Al4

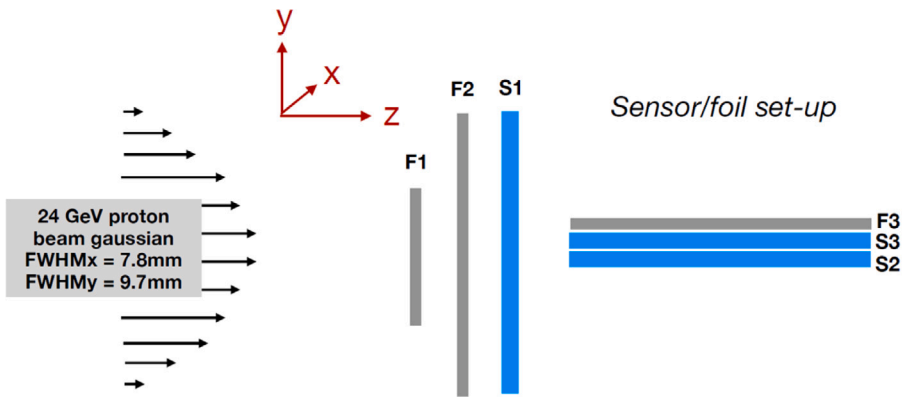

Fig. 6. Sketch of the irradiation experiment. Mini strip sensors are marked with S and aluminium foils with F. The size of the foil F1 is 0.5×0.5 cm^2 while F2 and F3 are 1×1 cm^2. The drawing is not to scale.

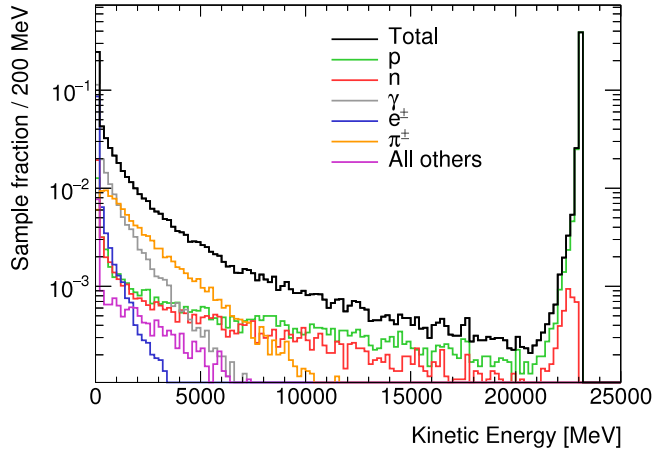

Fig. 7. Kinetic energy spectrum of particles hitting the sample in layer 11 (see Figs. 3 and 5).

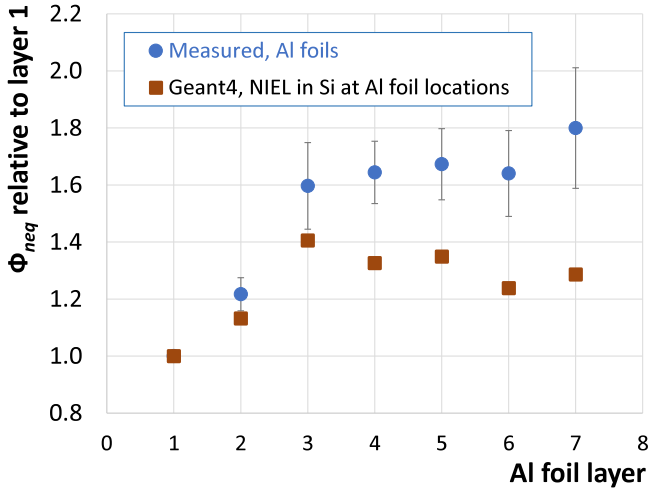

Fig. 8. Fluence relative to the fluence measured with the Al foil in layer 1 and fluences relative to the fluences in layer 1 calculated with the Geant4 simulation. Geant4 fluences were calculated for 1×1 cm^2 silicon, 300 μm thick, at the same location as Al foil. The measured values are averages for the measurements of four foils from four columns per layer and the error bars show the standard deviation of the four measurements.

Table 1
Table of estimated fluences for samples from four columns with different fluences and twelve layers at different angles in the setup. The Al foil used to estimate the fluence in the corresponding layer is specified (see Figs. 3 and 5).

Sensor layers	Angle [°]	Al#	Φ_{neq} Col. 1 [10^{14} cm^{-2}]	Φ_{neq} Col. 2 [10^{14} cm^{-2}]	Φ_{neq} Col. 3 [10^{14} cm^{-2}]	Φ_{neq} Col. 4 [10^{14} cm^{-2}]
1,5	90	Al1	0.9 ± 0.1	3.6 ± 0.3	5.5 ± 0.4	7.2 ± 0.5
2,6	12	Al1	1.1 ± 0.1	4.5 ± 0.5	6.8 ± 0.8	9.0 ± 1.1
3,4	6	Al1	1.1 ± 0.1	4.7 ± 0.6	7.1 ± 0.9	9.4 ± 1.1
7,8	1.5	Al1	1.1 ± 0.1	4.7 ± 0.6	7.1 ± 0.9	9.4 ± 1.1
9	90	Al3	1.5 ± 0.2	5.0 ± 0.7	8.8 ± 1.3	12.1 ± 1.8
10	1.5	Al4	1.5 ± 0.3	5.4 ± 0.8	9.2 ± 1.5	11.9 ± 1.8
11	90	Al5	1.6 ± 0.4	5.4 ± 0.8	9.2 ± 1.6	11.9 ± 1.8
12	1.5	Al6	1.6 ± 0.4	5.3 ± 0.8	8.8 ± 1.5	11.7 ± 2.1

near layer 10, Al5 near layer 11 and Al6 near the last layer 12 (see Figs. 3a and 5b). The fluences determined using these foils, by converting the measured radioactivity to fluence in the same way as for 24 GeV/c protons, are taken as the estimates of the fluences for the closest sensor layer. The Al foils were irradiated at an incidence angle of 90° while the sensors in layers 10 and 12 were irradiated at 1.5°. But the simulation in Fig. 5b shows that the effect of the angle is significantly smaller than for layers without G10 material, therefore no correction factor due to the angle was applied. The fluence uncertainty for these layers was roughly estimated as the difference between the fluence measured with the Al foil and the fluence calculated using Geant4. The Geant4-calculated fluence was obtained by multiplying the fluence measured with the Al foil in layer 1 by the relative fluence factor for each layer, as shown in Fig. 5b. A minimum uncertainty of 15% was set, corresponding to the average difference between measured and calculated values for these layers. The estimated fluences for individual samples in the twelve layers and four columns are summarized in Table 1.

The MD8 structures are silicon pad diodes with a 0.8×0.8 cm^2 surface area and a 300 μm active thickness. The current was measured with twelve MD8 diodes irradiated in columns 2 and 4 (see Fig. 3). The current was measured after annealing the diodes at 60 °C for 80 min. Measurements were made with MD8 diodes on a cold chuck, which stabilized the diode temperature at (5.0±0.1) °C. The measured currents were scaled to −20 °C using the effective silicon band gap energy of $E_g = 1.21$ eV [23]. This scaling was applied to enable easier comparison with the currents of mini strip detectors, which are measured at −20 °C in the charge collection measurement system. Fig. 9 shows the current at −20 °C and at 800 V reverse bias voltage as a function of the estimated fluences listed in Table 1.

The measured current is compared with the current expected for a fully depleted diode, calculated as $I = \alpha \cdot \Phi_{neq} \cdot V$, where $\alpha =$

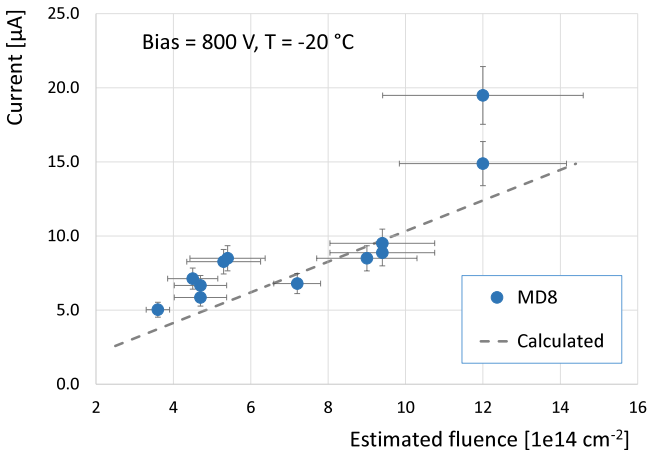

Fig. 9. The current measured with MD8 diodes at a reverse bias voltage of 800 V and scaled to temperature of −20 °C vs. the estimated fluence from Table 1. The dashed line shows the calculated current vs. fluence relation for a fully depleted MD8 diode.

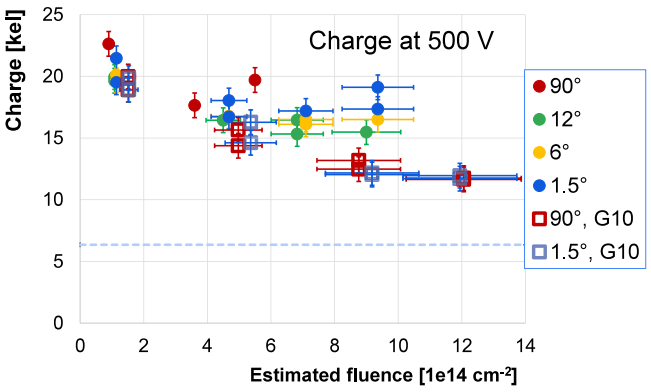

Fig. 10. The figure shows the collected charge (in the unit of kilo electrons [kel]) at 500 V reverse bias voltage vs. the fluence listed in Table 1. Different symbols and colours represent sensors at different angles in front of or behind blocks of G10 material. The horizontal dashed line shows a charge of 6350 electrons, which is the QA acceptance level for the ATLAS ITk strip detectors.

4×10^{-17} Acm^{-1} is the reverse current scaling factor at 20 °C [24], Φ_{neq} is the equivalent fluence and V is the depleted volume. The current values calculated with mentioned parameters were scaled to T = −20 °C using $E_g = 1.21$ eV in Fig. 9. A reverse bias voltage of 800 V was chosen because diodes were fully depleted at this voltage also at highest fluences. A reasonable agreement between the calculated and measured current is observed, indicating the accuracy of the fluence values estimated in Table 1.

4. Charge collection measurements

The charge collection of mini strip detectors was measured with electrons from a ^{90}Sr source using an ALiBaVa multi channel readout system employing the Beetle chip [25]. The mini strip detector was positioned between the ^{90}Sr source and a scintillator coupled to a photomultiplier. The electrons from the source hit the device-under-test at 90°. A trigger signal was provided by the signal from the scintillator generated by electrons from ^{90}Sr that crossed the strip detector. The trigger arrival time with respect to the Beetle clock was recorded with a precision of 1 ns and only events from a 10 ns wide time window, containing the peak of the amplifier output, were selected for measurements of the collected charge. The passage of electrons can induce signals in several neighbouring strips so the collected charge in an event was determined using a clustering algorithm. The distribution of cluster charges from several thousands of events was fitted with a Landau function convoluted with a Gaussian and the most probable value of the Landau function was defined as the collected charge at a given bias voltage. The uncertainty of the collected charge estimated in this way is about 1000 electrons [2]. The charge collection measurements shown in this work were made after annealing for 80 min at 60 °C. The measurements were taken with detectors cooled to −20 °C. See [26,27] for more detail about the measurement setup.

Fig. 10 shows the collected charge at 500 V reverse bias voltage measured with mini strip detectors irradiated at different angles with or without blocks of G10 material in the beam as a function of fluence. It can be seen in Fig. 10 that the collected charge is well above the QA acceptance level at all fluences in this experiment. The dependence of the collected charge on fluence is comparable with previous experiments [26] but with significant spread. It should be noted that the beam in IRRAD is very narrow so even small misalignments can have a significant impact on the fluence. Additionally, due to the narrow beam, the mini strip detectors are not irradiated uniformly. The position of the ^{90}Sr source, scintillator and collimators relative to the mini strip detector in the experimental setup may favour the part of the detector which was exposed to either higher or lower fluence. These uncertainties were not included when estimating the fluences.

The dependence of the collected charge on the irradiation angle is shown in Fig. 11. It can be seen that the collected charge for sensors with no G10 material between the samples and the beam in Fig. 11a is higher at 90° than at shallower angles for any fluence. This is expected due to geometrical effects in a beam with Gaussian shape of beam profile with a FWHM comparable to the dimension of the sample, as explained before. It can be seen that for angles 12° and lower the collected charge is slightly increasing as the angle decreases. This effect is currently not understood and parameters like proton beam profile, details of the position of samples in the beam should be known better to explain the feature.

Measurements for sensors with G10 material between the beam and the samples are shown in Fig. 11b. It can be seen that the collected charge is lower than in Fig. 11a for sensors irradiated in the same column because of the higher effective fluence. For the sensors in Fig. 11b no dependence on incidence angle is observed. This may be explained by secondary particles, which, according to measurements with Al foils in Fig. 8, might increase the effective fluence by up to 60%. These particles are generated at larger angles effectively broadening the beam making the irradiation more uniform and so reducing the influence of the angle. The Geant4 simulation in Fig. 5b also showed a much smaller effect of angle for sensors in layers 9, 10 than for layers 1, 2, 3 and 4.

Measurements shown in this section confirm that the material of the support structure and irradiation at shallow angle can cause a significant increase of the effective fluence, which results in significantly lower collected charge. It is therefore very likely that these effects contributed to low values of collected charge measured after irradiations at the IRRAD facility in 2021 and 2022.

4.1. Mixed irradiation

In the upgraded ATLAS experiment silicon strip detectors will be exposed to a mixture of neutrons and high energy charged hadrons [1,8]. More than 50% of the displacement damage in silicon strip detectors will be caused by neutrons and the rest by charged hadrons. In the most exposed part, the ITk strip detectors will accumulate $\Phi_{neq} \sim 5 \times 10^{14}$ cm^{-2} from charged hadrons while displacement damage equivalent to fluence $\Phi_{neq} \sim 6 \times 10^{14}$ cm^{-2} will come from neutrons. These are the expected radiation levels after 4000 fb^{-1} of integrated luminosity. The strip detectors were designed with a safety factor of 1.5 for a total fluence of $\Phi_{neq} = 1.6 \times 10^{15}$ cm^{-2} of which $\Phi_{neq} \sim 7 \times 10^{14}$ cm^{-2} comes from charged hadrons and $\Phi_{neq} \sim 9 \times 10^{14}$ cm^{-2} from neutrons [1,8].

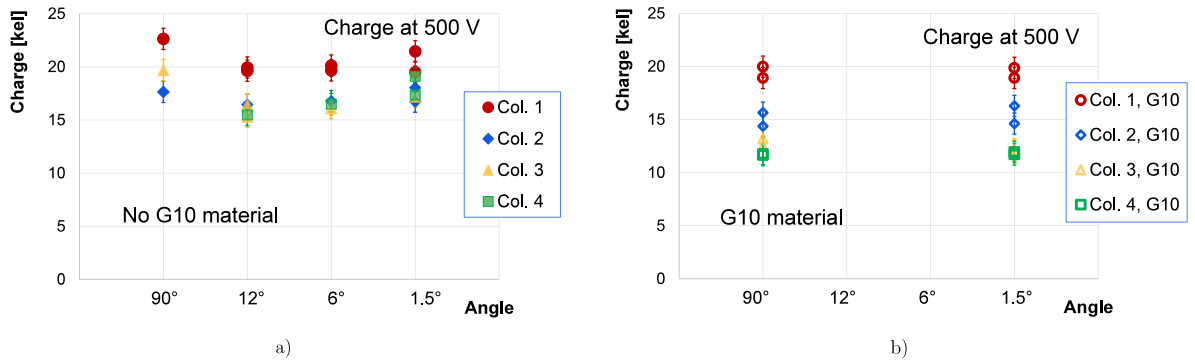

Fig. 11. (a) Collected charge vs. angle for sensor layers 1, 2, 3 and 4, without G10 material between the beam and sensors. Different colours are used for different target fluences (i.e. columns in the setup). (b) Collected charge measured with sensors at 90° and 1.5° in layers 9 and 10, with G10 material in the beam.

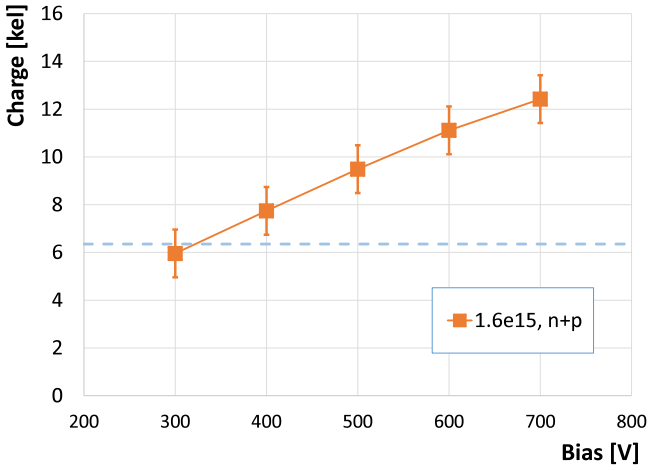

Fig. 12. Collected charge vs. bias voltage for mini strip detector irradiated with 24 GeV/c protons to $\Phi_{neq} \sim 7.2 \times 10^{14}$ cm^{-2} and with reactor neutrons to $\Phi_{neq} \sim 8.8 \times 10^{14}$ cm^{-2}, total fluence $\Phi_{neq} \sim 1.6 \times 10^{15}$ cm^{-2}. The collected charge was measured with a precision of 1000 electrons. The dashed line at 6350 electrons shows the minimal collected charge required at the bias of 500 V for ITk strip detectors.

To check the performance of the detector after irradiation with a mixture of particles, a sample that was exposed to $\Phi_{neq} \sim 7.2 \times 10^{14}$ cm^{-2} (see Table 1) at 24 GeV/c proton irradiation, was later also irradiated at the TRIGA reactor in Ljubljana [28,29] with neutrons to $\Phi_{neq} \sim 8.8 \times 10^{14}$ cm^{-2}. This resulted in a mixture close to that expected in the most exposed part of ITk strips. After irradiation with protons the sample was kept in the freezer. Irradiation with neutrons took less than 10 min and samples did not heat above ~40 °C [27] during this time so the annealing of damage caused by proton irradiation was not significant compared to the annealing for 80 min at 60 °C done before measurements. The charge collection measured as a function of bias voltage is shown in Fig. 12. It can be seen that the collected charge at 500 V is well above 6350 electrons, which is the minimum required for strip detectors in the ATLAS ITk.

4.2. Comparison with previous measurements

Fig. 13 shows a comparison of charge collection measurements as a function of fluence from a large number of irradiations with different particles and different versions of strip detectors. This includes measurements after irradiations with 24 GeV/c protons, in which collected charge below the acceptance level of 6350 electrons was measured near the design fluence of $\Phi_{neq} = 1.6 \times 10^{15}$ cm^{-2} (symbols A18 (PS2021) and A18 (PS2022) in Fig. 13). These measurements motivated the irradiation experiment described in this work aiming to identify the cause of the low collected charge and to ensure that the charge collection of ATLAS18 strip detectors will be sufficient at the highest fluences expected in the ITk.

5. Conclusion

In this work, collected charge was measured with ATLAS18 mini strip detectors irradiated with 24 GeV/c protons in a setup built to study the effects of material and irradiation angles. Measurements of Al foil activation and Geant4 simulations confirm that irradiation angles and material between the beam and the samples, which are specific to the sample holders, have to be considered to accurately estimate the fluence to which the samples were exposed in the narrow beam at the IRRAD facility. These effects were not considered in the 2021 and 2022 irradiations, which resulted in charge collection below the QA acceptance level. The amount of G10 material between the beam and the samples and shallow irradiation angles in the 2021 and 2022 setup (Fig. 1) could have caused similar effective fluence increase as observed in the 2023 experiment. Therefore, the actual fluence in those earlier measurements may have been underestimated by up to 60%. The results of mixed irradiation to the design fluence of $\Phi_{neq} = 1.6 \times 10^{15}$ cm^{-2} further confirm that ATLAS18 strip detectors will maintain sufficient charge collection efficiency in the radiation environment of ATLAS ITk up to highest fluences expected at the HL-LHC.

CRediT authorship contribution statement

I. Mandić: Writing – original draft. **V. Cindro:** Investigation. **M. Mikuž:** Investigation. **B. Novak:** Investigation. **P. Federičová:** Investigation. **R. Jirásek:** Investigation. **J. Kroll:** Investigation. **J. Kvasnička:** Investigation. **M. Mikeštíková:** Investigation. **P. Tůma:** Investigation. **V. Fadeyev:** Investigation. **Y. Unno:** Investigation. **E. Bach:** Investigation. **C. Fleta:** Investigation. **M. Ullan:** Investigation. **U. Soldevila:** Investigation. **R.S. Orr:** Investigation. **C.K. Mahajan:** Investigation. **S.K. Sridhar:** Investigation. **A.S. Chisholm:** Investigation. **I. Dawson:** Investigation.

Declaration of competing interest

The authors declare that they have no known competing financial interests or personal relationships that could have appeared to influence the work reported in this paper.

Acknowledgements

The authors would like to thank the crew at the TRIGA reactor in Ljubljana and the IRRAD facility at CERN for their help with the irradiations.

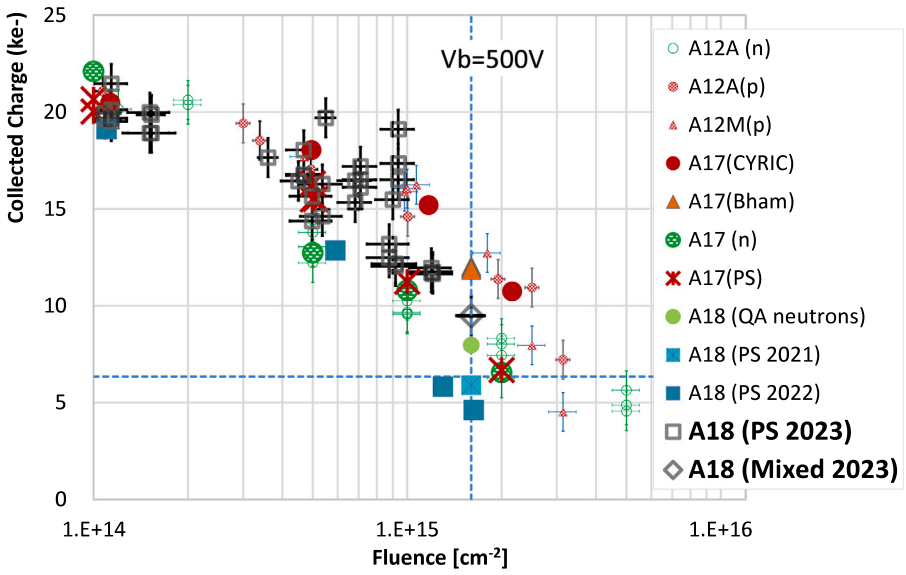

Fig. 13. Collected charge in the unit of kilo electrons [kel] at 500 V bias vs. Φ_{neq}. The graph shows a collection of results from various irradiation tests with neutrons (n in the legend), low energy protons (p, CYRIC, Bham) and with 24 GeV/c protons (PS) [26]. Measurements from the irradiation experiment described here are marked with A18(PS 2023) and A18(Mixed 2023).

The authors acknowledge the financial support from the Slovenian Research and Innovation Agency (research core funding No. P1-0135 and project No. J1-3032).

This work is part of the Spanish R&D grant PID2021-126327OB-C22 and grant PID2021-126327OB-C21, funded by MCIN/AEI/10.13039/501100011033 and by ERDF/UE. and part of the Spanish R&D grant PID2021-126327OB-C21, funded by MCIN/AEI/10.13039/501100011033/FEDER, UE.

This work was supported by the European Structural and Investment Funds and the Czech Ministry of Education, Youth and Sports of the Czech Republic via projects LM2023040 CERN-CZ, LTT17018 Inter-Excellence, and FORTE - CZ.02.01.01/00/22_008/0004632.

The work was supported by the USA Department of Energy, Grant DE-SC0010107.

This work was supported by the Canada Foundation for Innovation and the Natural Sciences and Engineering Research Council of Canada.

This project has received funding from the European Union's Horizon Europe Research and Innovation programme under Grant Agreement No 101057511 (EURO-LABS).

Data availability

Data will be made available on request.

References

[1] ATLAS Collaboration, TDR for the ATLAS Inner Tracker Strip Detector, CERN-LHCC-2017-005, ATLAS–TDR–025, 2017, URL https://cds.cern.ch/record/2257755.

[2] K. Hara, et al., Charge collection and field profile studies of heavily irradiated strip sensors for the ATLAS inner tracker upgrade, Nucl. Instr. Methods A 831 (2016) 181–188, http://dx.doi.org/10.1016/j.nima.2016.04.035.

[3] V. Cindro, et al., Measurement of the charge collection in irradiated miniature sensors for the upgrade of the ATLAS phase-II strip tracker, Nucl. Instr. Methods A 924 (2019) 153–159, http://dx.doi.org/10.1016/j.nima.2018.10.007.

[4] K. Hara, et al., Charge collection study with the ATLAS ITk prototype silicon strip sensors ATLAS17LS, Nucl. Instr. Methods A 983 (2020) 164422, http://dx.doi.org/10.1016/j.nima.2020.164422.

[5] E. Bach, et al., Analysis of the quality assurance results from the initial part of production of the ATLAS18 ITK strip sensors, Nucl. Instr. Methods A 1064 (2024) 169435, http://dx.doi.org/10.1016/j.nima.2024.169435.

[6] ROSE Collaboration, G. Lindström, et al., Radiation hard silicon detectors developments by the RD48 (ROSE) collaboration, Nucl. Instr. Methods A 466 (2001) 308, http://dx.doi.org/10.1016/S0168-9002(01)00560-5.

[7] V. Cindro, et al., Radiation damage in p-type silicon irradiated with neutrons and protons, Nucl. Instr. Methods A 599 (2009) 60–65, http://dx.doi.org/10.1016/j.nima.2008.11.007.

[8] ATLAS Phase II upgrade Radiation Maps. URL https://twiki.cern.ch/twiki/bin/view/AtlasPublic/RadiationSimulationPublicResults#Phase_II_Upgrade_Mar_2018.

[9] Y. Unno, et al., Specifications and pre-production of n^+-in-p large-format strip sensors fabricated in 6-inch silicon wafers, ATLAS18, for the inner tracker of the ATLAS detector for high-luminosity large hadron collider, JINST 18 (2023) T03008, http://dx.doi.org/10.1088/1748-0221/18/03/T03008.

[10] S. Hirose, et al., ATLAS ITk strip sensor quality assurance tests and results of ATLAS18 pre-production sensors, in: JPS Conf. Proc. of Vetex 2022, Vol. 42, 2024, 011017, http://dx.doi.org/10.7566/JPSCP.42.011017.

[11] F. Ravotti, et al., A new high-intensity proton irradiation facility at the CERN PS east area, in: Proceedings of TIPP 2014, Vol. PS(TIPP2014), 2024, p. 354, http://dx.doi.org/10.22323/1.213.0354.

[12] F. Ravotti, et al., The IRRAD proton irradiation facility control, data management and beam diagnostic systems: An outlook of the major upgrades beyond the CERN long shutdown 2, in: Proceedings ICALEPCS2019, New York, NY, USA, Vol. PS(TIPP2014), 2024, p. 354, http://dx.doi.org/10.18429/JACoW-ICALEPCS2019-WEPHA127.

[13] M. Glaser, F. Ravotti, M. Moll, Dosimetry assessments in the irradiation facilities at the CERN-PS accelerator, IEEE Trans. Nucl. Sci. 53 (2006) 2016, http://dx.doi.org/10.1109/TNS.2006.880569.

[14] P. Allport, et al., Experimental determination of proton hardness factors at several irradiation facilities, JINST 14 (2019) P12004, http://dx.doi.org/10.1088/1748-0221/14/12/P12004.

[15] A. Hermanne, et al., Reference cross sections for charged-particle monitor reactions, Nulcer Data Sheets 148 (2018) 338–382, http://dx.doi.org/10.1016/j.nds.2018.02.009.

[16] S. Agostinelli, et al., GEANT4 – a simulation toolkit, Nucl. Instr. Methods A 506 (3) (2003) 250–303, http://dx.doi.org/10.1016/S0168-9002(03)01368-8.

[17] The Shielding physics list. URL https://geant4.web.cern.ch/documentation/dev/plg_html/PhysicsListGuide/reference_PL/Shielding.html.

[18] A. Vasilescu, G. Lindström, Displacement damage in silicon, 2000, URL https://rd50.web.cern.ch/niel/.

[19] M. Huhtinen, P.A. Aarnio, Pion induced displacement damage in silicon devices, Nucl. Instr. Methods A 335 (3) (1993) 580–582, http://dx.doi.org/10.1016/0168-9002(93)91246-J.

[20] G.P. Summers, et al., Damage correlations in semiconductors exposed to gamma, electron and proton radiations, IEEE Trans. Nucl. Sci. 40 (6) (1993) 1372–1379, http://dx.doi.org/10.1109/23.273529.

[21] A.Yu. Konobeyev, Yu.A. Korovin, Neutron displacement cross-sections for structural materials below 800 MeV, J. Nucl. Mater. 186 (2) (1992) 117, http://dx.doi.org/10.1016/0022-3115(92)90328-I.

[22] S. Yang, et al., ^{22}Na activation level measurements of fused silica rods in the LHC target absorber for neutrals compared to simulations, Phys. Rev. Accel. Beams 25 (2022) 091001, http://dx.doi.org/10.1103/PhysRevAccelBeams.25.091001.

[23] A. Chilingarov, Temperature dependence of the current generated in Si bulk, JINST 8 (2013) P10003, http://dx.doi.org/10.1088/1748-0221/8/10/P10003, 13.

[24] M. Moll, E. Fretwurst, G. Lindström, Leakage current of hadron irradiated silicon detectors – material dependence, Nucl. Instr. Methods A 426 (1999) 87, http://dx.doi.org/10.1016/S0168-9002(98)01475-2.

[25] R. Marco-Hernández, A portable readout system for silicon microstrip sensors, Nucl. Instr. Methods A 623 (2010) 207–209, http://dx.doi.org/10.1016/j.nima.2010.02.197.

[26] K. Hara, et al., Charge collection study with the ATLAS ITk prototype silicon strip sensors ATLAS17LS, Nucl. Instr. Methods A 983 (2020) 164422, http://dx.doi.org/10.1016/j.nima.2020.164422.

[27] V. Cindro, et al., Measurement of the charge collection in irradiated miniature sensors for the upgrade of the ATLAS phase-II strip tracker, Nucl. Instr. Methods A 924 (2019) 153, http://dx.doi.org/10.1016/j.nima.2018.10.007.

[28] L. Snoj, G. Žerovnik, A. Trkov, Computational analysis of irradiation facilities at the JSI TRIGA reactor Measurement, Appl. Radiat. Isot. 70 (2012) 483, http://dx.doi.org/10.1016/j.apradiso.2011.11.042.

[29] K. Ambrožič, G. Žerovnik, L. Snoj, Computational analysis of dose rates at the JSI TRIGA reactor irradiation facilities, Appl. Radiat. Isot. 130 (2017) 140, http://dx.doi.org/10.1016/j.apradiso.2017.09.022.